PHILOSOPHICAL TRANSACTIONS OF THE ROYAL SOCIETY A MATHEMATICAL, PHYSICAL & ENGINEERING SCIENCES

One-Electron Theory of Nonlinear Refraction

B. S. Wherrett

Phil. Trans. R. Soc. Lond. A 1984 **313**, 213-220
doi: 10.1098/rsta.1984.0098

Phil. Trans. R. Soc. Lond. A **313**, 213–220 (1984)
Printed in Great Britain

One-electron theory of nonlinear refraction

By B. S. Wherrett

Department of Physics, Heriot-Watt University, Riccarton, Currie, Edinburgh EH14 4AS, U.K.

The design of optically bistable cavities for low-power switching requires an understanding of the variation of nonlinearities in refractive index with material, temperature, wavelength and cavity parameters. Analytic expressions, suitable for scaling, are discussed. The connections between the giant nonlinearities under current investigation and the nonlinear optical mixing processes studied since the 1960s are reviewed and the self-consistent semiconductor optical bistability problem is summarized.

1. Introduction

The key to recent advances in the application of optical bistability has been the realization that semiconductor materials exist in which the intensity dependence of the refractive index is large enough to produce bistable characteristics at low power levels and in small samples.

The demands upon the nonlinearity for bistable operation are determined by reference to the transmission of a Fabry–Perot cavity (Miller 1981; Wherrett 1984). One can define a critical switching intensity, I_c, below which bistability and hysteresis cannot be achieved and above which it can occur for suitable initial conditions.

Given an internal irradiance I and associated contribution to the refractive index, $\Delta n(I)$, then I_c can be determined in terms of a material factor and a cavity factor. Optimizing the cavity reflectivities and length to minimize I_c one concludes that a Δn of order 10^{-3} is necessary to achieve bistability in semiconductors. Concentrating on the case $\Delta n(I) = n_2 I$, one requires for switching at frequency ω in a medium of linear refractive index n:

$$\Delta n(I) = n_2 I \approx nc\alpha/3\omega. \tag{1}$$

The coefficient n_2 is directly proportional to the real part of the third-order optical susceptibility, $\chi^{(3)}(\omega, -\omega, \omega)$, such that for switching at, say, 1 kW cm^{-2} one requires:

$$\mathrm{Re}\,\chi^{(3)} = (n^2 c/4\pi\omega^2)\, n_2 \approx 10^{-3}\ \text{e.s.u.}\dagger \tag{2}$$

2. First estimates

A quasi-dimensional analysis provides the simplest, first assessment of $\chi^{(3)}$. Interest lies in near-resonance situations where specific optical transitions dominate the nonlinearity. Consider N discrete atoms per unit volume, characterized by two-level systems of energy difference E_{10} and a transition dipole-moment er_{10}. Introducing the electromagnetic field interaction three times to attain a polarization, $\langle Ner \rangle$, third-order in the field, one must obtain

$$\chi^{(3)}_{\mathrm{atom}} \propto N e^4 r_{10}^4 E_{10}^{-3} F(\hbar\omega/E_{10}). \tag{3}$$

† 1 e.s.u. = 1 cm^3 erg^{-1} $\equiv 1.4 \times 10^{-8}$ m^2 V^{-2}.

The dimensionless function F is as yet unspecified; if we were to set F equal to unity then a characteristic gaseous $\chi^{(3)}$ of a mere 10^{-18} e.s.u. may be obtained.

Considerable improvement occurs for the semiconductor case. Now the density of atoms is replaced by a sum over semiconductor $\boldsymbol{k}$-states per unit volume and E_{10} is replaced by the k-dependent energy gap, $E(k) = E_g + \hbar^2 k^2/2m_r$. The reduced effective mass, m_r, is determined from the band interaction Hamiltonian ($H' = (\hbar/m)\,\boldsymbol{k}\cdot\boldsymbol{p}$), which is formally very similar to the radiative interaction ($H' = \mathrm{i}(e/m\omega)\,\boldsymbol{\mathscr{E}}\cdot\boldsymbol{p}\exp(-\mathrm{i}\omega t) + \mathrm{c.c.}$). Here $\boldsymbol{\mathscr{E}}$ is the electric field vector and $\boldsymbol{p}$ the momentum operator. If we introduce the Kane P-parameter, which is directly proportional to the momentum matrix element for interband transitions ($P = (\hbar/m)\,|p_{cv}|$), then E_g, P and $\hbar$ form a suitable set of parameters for dimensional analysis, leading to

$$\chi^{(3)}_{\text{semiconductor}} \propto e^4 P E_g^{-4} F(\hbar\omega/E_g). \tag{4}$$

For a small-gap semiconductor $\chi^{(3)} \approx F \times 10^{-9}$ e.s.u. Over the range of semiconductors P is essentially constant and the linear refractive index varies by a factor of less than two over most, whereas the band gap can vary by a factor of ten or more. Thus the E_g^{-4} dependence is expected to dominate any scaling. The factor F must be considered if magnitudes such as required for bistability are to be achieved. To do so one must recognize that F will contain resonance enhancement factors. The likelihood of a large F is seen by considering figure 1. This shows

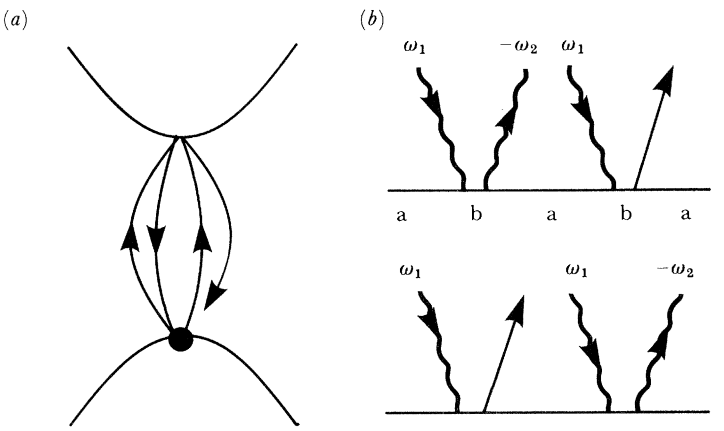

FIGURE 1. The most resonant contribution to nonlinear refraction (*a*) Four-stage transition scheme; (*b*) time-ordering diagrams ($\omega_2 = \omega_1$ for refraction).

a four-stage transition scheme and two associated time-ordering diagrams, describing the three electromagnetic field interactions and the emission of a photon via the generated polarization. The corresponding mathematical contributions to $\chi^{(3)}$ will be proportional to the times for which each intermediate state can exist (Δt). In turn each Δt is inversely proportional to the energy mismatch between the intermediate (virtual) state of the system, and the initial state ($\Delta t \approx \hbar/\Delta E$). But for the chosen schemes the second intermediate state has precisely the same energy as the initial state. Thus $\Delta E = 0$ and the contributions to $\chi^{(3)}$ diverge to infinity. As we would expect, in practice the divergence is prohibited; nevertheless some nine orders of magnitude increase in $\chi^{(3)}$ will be derived from F (§4).

PHILOSOPHICAL TRANSACTIONS OF THE ROYAL SOCIETY A MATHEMATICAL, PHYSICAL & ENGINEERING SCIENCES

3. Observations and interpretations

Franken & Ward recognized the existence of an intensity dependence of refraction in 1963, commenting in their theoretical paper that the phenomenon had 'not yet been observed', although in 1962 frequency-mixing processes in calcite had been observed by Terhune *et al.*, with $\chi^{(3)}$ magnitudes around 10^{-15} e.s.u. The first refractive nonlinearities (Mayer & Gires 1964; Maker *et al.* 1964), observed in liquids, gave values up to 10^{-12} e.s.u.

One must turn to $(2\omega_1-\omega_2)$ four-photon mixing experiments for the earliest relevant semiconductor studies. This mixing is close to being a nonlinear refraction process and would be so if ω_2 were adjusted to be equal to ω_1. In the large gap material CdS, Maker & Terhune (1965) observed a correspondingly small $\chi^{(3)}$ of 5×10^{-12} e.s.u. With the invention of the infrared CO_2 laser, however, Patel *et al.* (1966) was able to study small gap semiconductors, achieving 8×10^{-10} e.s.u. in InSb with ω_1, $\omega_2\approx1000$, 1100 cm^{-1} respectively (the InSb band edge corresponds to approximately 1900 cm^{-1}).

Between 1965 and 1975 interest in nonlinear refraction centred on self-focusing studies, primarily in liquids. Here one is concerned with the spatial refractive index change brought about by an intense Gaussian beam and the resulting beam trapping and filamentation. The physical origin of self-focusing nonlinearities has been predominantly the molecular-orientational Kerr effect, inappropriate in solids, although as long ago as 1966 Javan & Kelley suggested that the saturation of anomalous dispersion in gases should lead to high Δn values.

Renewed interest in semiconductor nonlinear refraction came about as a culmination of several independent investigations. The first was the prediction of Szöke *et al.* (1969) that optical bistability should be possible for a saturating medium with feedback, and Gibbs's demonstration (1976) that optical bistability could be observed (in sodium vapour) but that the origin was dispersive. The second was the growing interest, since the transient holography work of Woerdman & Bolger (1969), in the dynamic refractive index gratings established when non-collinear laser beams interfere across a semiconductor sample. The diffraction of a third beam allows one to study the dynamics of the excited carriers that produced the index grating (Jarasiunas & Vaitkus 1974) or to achieve phase conjugation (Bergmann *et al.* 1978). Thirdly the 1970s were the era of the spin-flip Raman laser. In this instrument one is pumping a semiconductor (albeit in a high magnetic field) at a frequency just below the band gap (Dennis *et al.* 1972). At the time $\chi^{(3)}$ refractive index effects associated with the Raman gain were known to be present, causing mode-pulling, and the observed break-up of the transmitted pump-beam spatial profile was likely to have been due to nonlinear refraction.

It was not until the late 1970s, however, that the giant nonlinearities required for bistability were recognized. Thus, at continuous-wave (c.w.) CO-laser power levels, transmitted beam profile studies and analysis for InSb (Miller *et al.* 1978; Weaire *et al.* 1979) produced $\chi^{(3)}$ values up to 10^{-2} e.s.u. for frequencies just below the band edge, as have studies of phase conjugation and degenerate four-wave mixing in cadmium mercury telluride (Jain 1982). Finally, in 1979 reports were made of the first semiconductor optical bistability experiments (Gibbs *et al.* 1979; Miller *et al.* 1979) with $\chi^{(3)}$ values of 10^{-5} to 10^{-4} e.s.u. in GaAs and 1 e.s.u. in InSb.

A number of theoretical models have been used to interpret the various observations discussed above. Early mixing work was explained in terms of (i) free-carrier non-parabolicity (Wolff & Pearson 1966) and (ii) virtual interband transitions (Jha & Bloembergen 1968; Wynne 1969). Giant nonlinear refraction has been discussed (iii) using a direct saturation model (Miller

et al. 1980), (iv) in terms of a dynamic Burstein–Moss effect (Wherrett & Higgins 1982; Moss 1980), (v) as a free carrier plasma effect (Jain & Klein 1980) and (vi) as an enhanced non-parabolicity effect (Khan *et al.* 1981). In addition a many-body treatment has been made by Haug and coworkers (Koch & Haug 1981; Haug & Schmitt-Rink, this symposium).

These models, and the range of experimental data, lead one to pose the following questions: How do the models relate? What resonance factors should one use? Can the eleven orders of magnitude between the mixing $\chi^{(3)}$, 10^{-11} e.s.u. in CdS and the 1 e.s.u. refractive $\chi^{(3)}$ in InSb be bridged smoothly? And how should one best calculate the giant nonlinear indices now being studied?

4. Unification of theoretical models

In the non-parabolicity model one considers the momentum dependence of the effective mass of free carriers. As a result, in an applied electric field $\mathscr{E}$ the carrier velocities contain terms in $\mathscr{E}^3$ so that the conductivity (and susceptibility) contain third-order terms. In essence one obtains

$$\chi^{(3)} \approx +N_0 e^4 p^4 E_g^{-7} F(E_F/E_g), \tag{5}$$

where E_F is the carrier Fermi energy. N_0 is the initial density of carriers and there is no need to mention interband transitions in the theoretical approach.

By contrast, starting with four-stage virtual interband transitions for mixing at $(2\omega_1-\omega_2)$ one obtains a non-diverging expression for $\chi^{(3)}$ dominated by the processes shown in figure 1*b*. Summing over the two schemes there is a partial cancellation of terms, following which ω_2 can be set equal to ω_1 without producing the divergence problem discussed earlier (Wherrett 1983). As a result, for N_0 electrons at the bottom of the conduction band,

$$\chi^{(3)}_{N_0} \approx N_0 e^4 \frac{P^4}{E_g^7}\left[\frac{E_g}{E_g-\hbar\omega}\right]^3. \tag{6}$$

Expression (5) is regained in the limit $\hbar\omega \ll E_g$ showing that the non-parabolicity model is based on interband processes. For a full valence band and empty conduction band this virtual transition scheme model gives

$$\chi^{(3)} \approx -e^4 \frac{P}{E_g^4}\left[\frac{E_g}{E_g-\hbar\omega}\right]^{\frac{3}{2}}. \tag{7}$$

Note that this has precisely the scaling form predicted by dimensional analysis; also $\chi^{(3)}$ displays a minus three-halves resonance behaviour and is negative. The latter is significant experimentally because a negative nonlinear refraction leads to beam defocusing, which is stable by comparison with the catastrophic self-focusing.

The efficiency of resonance enhancement of virtual processes is demonstrated by recent $(2\omega_1-\omega_2)$-mixing observations in InSb (MacKenzie *et al.* 1984). As one approaches the band edge $\chi^{(3)}$ values up to 10^{-6} e.s.u. have been observed, some three orders of magnitude greater than are observed with mid-gap frequencies. These values are, however, still six orders of magnitude smaller than the refractive $\chi^{(3)}$ near resonance. To bridge this gap one must reduce the 4 cm^{-1} difference in ω_1 and ω_2 used for the above mixing experiment, thereby detecting the effect of real (rather than virtual) excitation of carriers.

By introducing two effective scattering times one can make the link between the virtual transition picture and the plasma or Burstein–Moss pictures. By analogy with a two-level system

PHILOSOPHICAL TRANSACTIONS OF THE ROYAL SOCIETY A MATHEMATICAL, PHYSICAL & ENGINEERING SCIENCES

consider the optically coupled valence and conduction states, lying at the same $\boldsymbol{k}$. Describe intraband scattering, due for example to electron–electron and electron–phonon interactions, by a damping or dephasing lifetime T_2. Describe interband recombination by a time T_1. Real (long-term) excitation becomes important for $(E_g/\hbar-\omega) \lesssim 1/T_2$ and, in mixing, for $|\omega_1-\omega_2| \lesssim 1/T_1$. The same time-ordered diagrams (figure 1*b*) dominate $\chi^{(3)}$, which can be calculated by using density matrix theory with the essential result

$$\chi^{(3)} \approx \chi^{(3)}_{\text{virtual}}\, T_1/T_2. \tag{8}$$

Introduction of T_2 and T_1 is the basis of the direct saturation model of the nonlinearity. The T_2 lifetime can also be used, phenomenologically, to describe the band-tail absoption that must be present for real excitation:

$$\alpha_{\text{tail}} \approx \frac{e^2}{n\hbar cP}\frac{1}{T_2}\left[\frac{E_g}{E_g-\hbar\omega}\right]^{\frac{1}{2}}. \tag{9}$$

By fitting to the observed tail one obtains an effective T_2 (Higgins 1983). Alternatively one can re-express $\chi^{(3)}$ directly in terms of α, or Δn in terms of the equilibrium excited-carrier concentration $(\Delta N = \alpha I T_1/\hbar\omega)$:

$$\chi^{(3)} \approx -\frac{e^2P^2}{E_g^4} nc\alpha T_1\left[\frac{E_g}{E_g-\hbar\omega}\right] \tag{10a}$$

or

$$\Delta n \approx \frac{-e^2P^2}{nE_g^3}\Delta N\left[\frac{E_g}{E_g-\hbar\omega}\right]. \tag{10b}$$

Within small factors precisely these results are also achieved in the Burstein–Moss and plasma models. The differences lie only in that a different distribution of excited carriers is described in each model. Figure 2 shows such conduction electron distributions schematically. Under direct saturation the carriers partly populate the optically coupled states and remain in these states, those nearest resonance being the most strongly saturated (figure 2*a*). In the Burstein–Moss model it is recognized that T_2 scattering will thermalize the carriers (figure 2*b*). The plasma model is the low-temperature limit to the Burstein–Moss description (figure 2*c*). In the

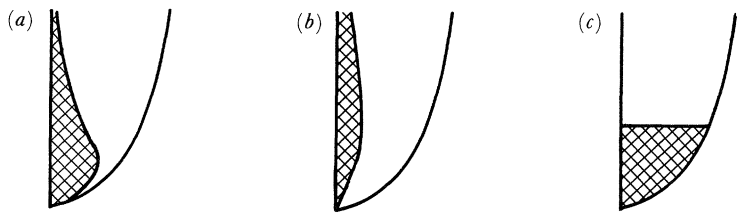

FIGURE 2. Excited conduction electron distribution for (*a*) direct saturation (*b*) the Burstein–Moss model and (*c*) Burstein–Moss at zero temperature or the plasma model.

latter two models the excitation and refraction may be treated separately. One calculates N at equilibrium, allows a thermal distribution to establish, then calculates the refractive index change due to this change in electron distribution among the bands. One obtains a nonlinear index only through the intensity dependence of N. The conventional Burstein–Moss effect is a shift of the effective band edge for a doped material. In the dynamic Burstein–Moss picture

one thinks of the radiative generation of carriers causing a dynamic edge-shift and of the nonlinear refraction as a result of the absorption change. In the plasma picture the N carriers have a plasma frequency ω_p and near the semiconductor band edge one has a dielectric response

$$\epsilon \approx \epsilon_\infty \left(1 - \frac{\omega_p^2}{\omega^2} \frac{E_g^2}{E_g^2 - \hbar^2\omega^2}\right). \tag{11}$$

Equation (10*b*) is regained on analysis of this result, demonstrating once again that the band-edge enhancement in (11) is merely a recognition of the blocking of *interband* transitions due to the carrier plasma.

The Burstein–Moss and plasma pictures are more flexible than the direct saturation model as they can accommodate any interband absorption source (direct, two-photon, etc.) and any recombination process (via traps as described by T_1, or via radiative or Auger recombination). Furthermore the use of a Kramers–Kronig analysis on the absorption change due to the thermal carrier distribution enables any temperature to be considered. Thus for example in the Boltzmann high-temperature limit (Miller 1981),

$$\chi^{(3)} \approx \frac{e^2P^2}{E_g^3 k_B T} nc\alpha T_1 J\left(\frac{k_B T}{E_g - \hbar\omega}\right). \tag{12}$$

These advantages lead us to the self-consistent approach to the Δn problem.

5. The self-consistent semiconductor optical bistability problem

Figure 3 demonstrates the calculations necessary for c.w., plane-wave, dispersive optical bistability in a semiconductor cavity. Starting at the left hand side one has a semiconductor characterized by a refractive index n, interband adsorption α_i and a parasitic absorption (due for example to the created free-carriers) α_p. For an incident irradiance I_1 at frequency ω one determines the internal irradiance $I(\omega)$ and the transmitted or reflected (or both) irradiances: this is the cavity feedback problem.

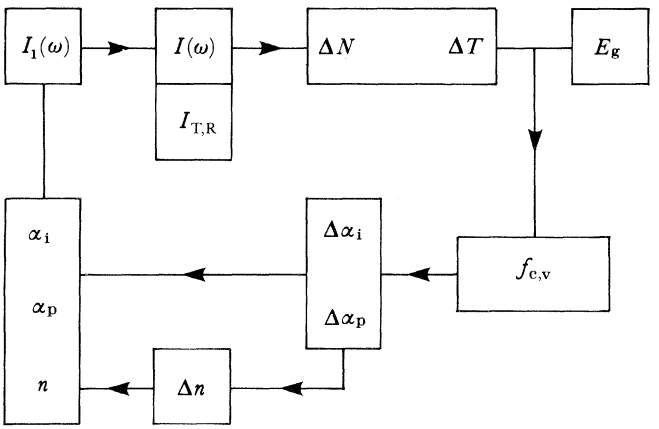

Figure 3. The semiconductor optical bistability self-consistency problem.

The internal irradiance generates ΔN carriers: the recombination problem; simultaneously there may be a change of sample temperature, ΔT. As a consequence the band edge and structure will alter, directly through ΔT and via many-body effects (gap renormalization). Assuming separate thermalization within the conduction band and the valence band one

calculates the new carrier distributions f_c and f_v and, given an understanding of all absorption processes, both absorption changes $\Delta\alpha_i$ and $\Delta\alpha_p$ at all frequencies may be calculated. A Kramers–Kronig-type transformation will then produce the refractive index change Δn at the frequency of interest (ω). All three of $\Delta\alpha_i$, $\Delta\alpha_p$ and Δn must then be cycled around this loop self-consistently.

The linear proportionality of Δn to I will be true only under special conditions (low intensities, small carrier densities). Further, one must in practice consider time-dependent effects (switching, transients, pulsed operation) and spatially dependent effects (beam diffraction and lensing, and carrier diffusion) as discussed in following articles in this symposium. Nevertheless the $\chi^{(3)}$ or n_2 approximation has been demonstrated to be valid for certain experiments (Miller *et al.* 1981; Garmire *et al.*, this symposium). Figure 4 shows just such a case, and shows that a fit to n_2 (solid line) can be achieved within a description in which the absorption (modelled by a T_2-tail) is allowed to saturate self-consistently due to a thermal carrier distribution. This technique allows us to generate *effective* T_2 and T_1 times of around 10 ps and 1 μs respectively, a ratio $T_1/T_2 \approx 10^5$.

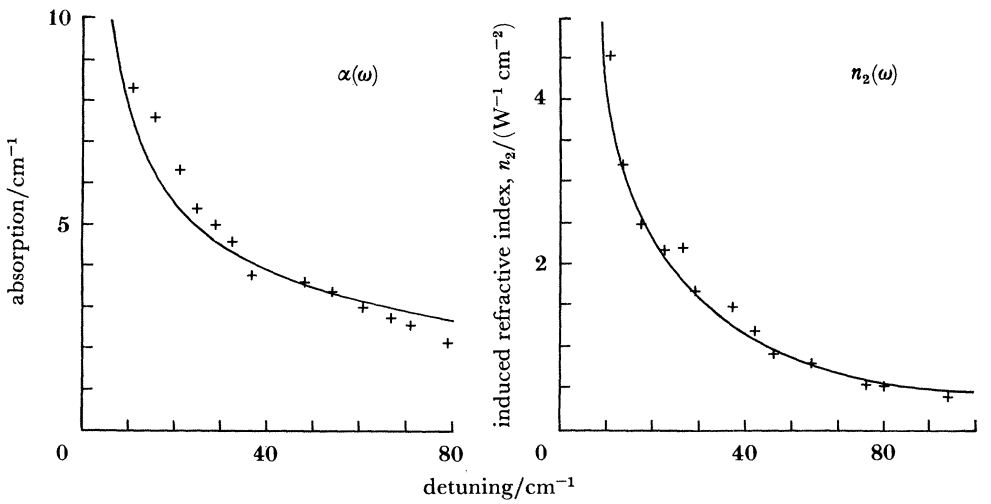

FIGURE 4. Self-consistent calculations for n_2 (Higgins 1983) fitted to the experimental data of Miller (1979) indicating an effective T_1/T_2 of 10^5 (see text).

6. CONCLUSION

In conclusion it can be demonstrated that the various models for $\chi^{(3)}$ and Δn discussed above are all based on interband carrier excitation (virtual or long term) and that one can scale n_2 essentially as

$$n_2 \approx \frac{-e^4}{c}\frac{P}{n^2E_g^4}\left[\frac{E_g}{E_g-\hbar\omega}\right]^{\frac{3}{2}}\frac{T_1}{T_2}. \tag{13}$$

The eleven orders of magnitude increase from $\chi^{(3)}(\omega_1, -\omega_2, \omega_1)$ in CdS to $\chi^{(3)}(\omega, -\omega, \omega)$ in InSb are bridged by moving to smaller gap material ($\times 10^2$), approaching resonance ($\times 10^3$), and equating the frequencies ω_2 and ω_1 ($\times 10^5 - 10^6$). Finally I give as an example in the high temperature limit an expression for the critical bistability switching intensity,

$$I_c \approx \frac{\hbar c}{e^2}\frac{n^2E_g^2}{P^2T_1}k_B\,T\,J^{-1}\left(\frac{k_B\,T}{E_g-\hbar\omega}\right)f(\text{cavity}). \tag{14}$$

This expression indicates the considerations of material, temperature, frequency and cavity parameters that must be taken into account to optimize for low-intensity switching.

This work was done in the framework of an operation launched by the Commission of the European Community under the experimental phase of the European Community Stimulation Action (1983–85).

References

Bergmann, E. E., Bigio, I. J., Feldman, B. J. & Fisher, R. A. 1978 *Optics Lett.* **3**, 82.
Dennis, R. B., Pidgeon, C. R., Smith, S. D., Wherrett, B. S. & Wood, R. A. 1972 *Proc. R. Soc. Lond.* A **331**, 203.
Franken, P. A. & Ward, J. F. 1963 *Rev. mod. Phys.* **35**, 23.
Gibbs, H. M., McCall, S. L. & Venkatesan, T. N. C. 1976 *Phys. Rev. Lett.* **36**, 1135.
Gibbs, H. M., McCall, S. L., Venkatesan, T. N. C., Passner, A., Gossard, A. C. & Weigmann, W. 1979 *Solid St. Commun.* **30**, 271.
Higgins, N. A. 1983 Ph.D. thesis, Heriot-Watt University.
Jain, R. K. 1982 *Opt. Engng* **21**, 199.
Jain, R K. & Klein, M. B. 1980 *Appl. Phys. Lett.* **37**, 1.
Jarasuinas, K. & Vaitkus, J. 1974 *Physica Status Solidi* A **23**, K19.
Javan, A. & Kelley, P. L. 1966 *IEEE Jl Quantum Electron.* **QE-2**, 470.
Jha, S. S. & Bloembergen, N. 1968 *Phys. Rev.* **171**, 891.
Khan, M. A., Bogant, T. J., Kruse, P. W. & Ready, J. F. 1981 *Optics Lett.* **5**, 469.
Koch, S. W. & Haug, H. 1981 *Phys. Rev. Lett.* **46**, 450.
MacKenzie, H. A., Al-Attar, H. & Wherrett, B. S. 1984 *J. Phys.* B **17**, 2141.
Maker, P. D. & Terhune, R. W. 1965 *Phys. Rev.* A **137**, 801.
Maker, P. D., Terhune, R. W. & Savage, C. M. 1964 *Phys. Rev. Lett.* **12**, 507.
Mayer, G. & Gires, F. 1964 *C.r. hebd. Seanc. Acad. Sci., Paris* **258**, 2039.
Miller, D. A. B. 1979 Ph.D. thesis, Heriot-Watt University.
Miller, D. A. B. 1981 *IEEE Jl Quantum Electron.* **QE-17**, 306.
Miller, D. A. B., Mozolowski, M. H., Miller, A. & Smith, S. D. 1978 *Optics Commun.* **27**, 133.
Miller, D. A. B., Seaton, C. T., Prise, M. E. & Smith, S. D. 1981 *Phys. Rev. Lett.* **47**, 197.
Miller, D. A. B., Smith, S. D. & Johnston, A. 1979 *Appl. Phys. Lett.* **35**, 658.
Miller, D. A. B., Smith, S. D. & Wherrett, B. S. 1980 *Optics Commun.* **35**, 221.
Moss, T. S. 1980 *Physica Status Solidi* B **101**, 555.
Patel, C. K. N., Slusher, R. E. & Fleury, P. A. 1966 *Phys. Rev. Lett.* **17**, 1010.
Szöke, A., Damen, V., Goldhar, J. & Kurnit, N. A. 1969 *Appl. Phys. Lett.* **15**, 376.
Terhune, R. W., Maker, P. D. & Savage, C. M. 1962 *Phys. Rev. Lett.* **8**, 401.
Weaire, D. L., Wherrett, B. S., Miller, D. A. B. & Smith, S. D. 1979 *Optics Lett.* **4**, 831.
Wherrett, B. S. 1983 *Proc. R. Soc. Lond.* A **390**, 373.
Wherrett, B. S. 1984 *IEEE Jl Quantum Electron.* **QE-20**, 646.
Wherrett, B. S. & Higgins, N. A. 1982 *Proc. R. Soc. Lond.* A **379**, 67.
Woerdman, J. P. & Bolger, B. 1969 *Phys. Lett.* A **30**, 164.
Wolff, P. A. & Pearson, G. A. 1966 *Phys. Rev. Lett.* **17**, 1015.
Wynne, J. J. 1969 *Phys. Rev.* **138**, 1296.

PHILOSOPHICAL TRANSACTIONS OF THE ROYAL SOCIETY A MATHEMATICAL, PHYSICAL & ENGINEERING SCIENCES